

Paleoceanography and Paleoclimatology*



RESEARCH ARTICLE

10.1029/2022PA004600

Key Points:

- Different areas of the Southern Ocean (SO) show different consistency between model simulations and proxy data
- Regions along the edges of the modern day SO gyres show the least consistency between models and proxy data
- Inclusion of Heinrich 11 meltwater forcing improves the match between model simulations and proxy data

Supporting Information:

Supporting Information may be found in the online version of this article.

Correspondence to:

M. Chadwick,
m.chadwick@cornwall-insight.com

Citation:

Chadwick, M., Sime, L. C., Allen, C. S., & Guarino, M.-V. (2023). Model-data comparison of Antarctic winter sea-ice extent and Southern Ocean sea-surface temperatures during Marine Isotope Stage 5e. *Paleoceanography and Paleoclimatology*, 38, e2022PA004600. <https://doi.org/10.1029/2022PA004600>

Received 14 DEC 2022
Accepted 15 MAY 2023





Author Contributions:

Conceptualization: L. C. Sime, C. S. Allen
Data curation: M. Chadwick, M.-V. Guarino
Formal analysis: M. Chadwick, M.-V. Guarino
Funding acquisition: L. C. Sime, C. S. Allen
Investigation: M. Chadwick, M.-V. Guarino
Methodology: M. Chadwick, C. S. Allen, M.-V. Guarino
Project Administration: L. C. Sime, C. S. Allen
Resources: M. Chadwick, C. S. Allen

© 2023. The Authors.

This is an open access article under the terms of the [Creative Commons Attribution License](https://creativecommons.org/licenses/by/4.0/), which permits use, distribution and reproduction in any medium, provided the original work is properly cited.

Model-Data Comparison of Antarctic Winter Sea-Ice Extent and Southern Ocean Sea-Surface Temperatures During Marine Isotope Stage 5e

M. Chadwick^{1,2,3} , L. C. Sime¹ , C. S. Allen¹ , and M.-V. Guarino^{1,4} 

¹British Antarctic Survey, Cambridge, UK, ²Ocean and Earth Science, University of Southampton, Southampton, UK, ³Now at Cornwall Insight, Norwich, UK, ⁴Earth System Physics Section, International Centre for Theoretical Physics, Trieste, Italy

Abstract Marine Isotope Stage (MIS) 5e (130–116 ka) represents a “laboratory” for evaluating climate model performance under warmer-than-present conditions. Climate model simulations for MIS 5e have previously failed to produce Southern Ocean (SO) sea-surface temperatures (SSTs) and sea-ice extent reconstructed from marine sediment core proxy records. Here we compare state of the art HadGEM3 and HadCM3 simulations of Peak MIS 5e SO summer SSTs and September sea-ice concentrations with the latest marine sediment core proxy data. The model outputs and proxy records show the least consistency in the regions located near the present-day SO gyre boundaries, implying the possibility that model simulations are currently unable to fully realize changes in gyre extent and position during MIS 5e. Including Heinrich 11 meltwater forcing in Peak MIS 5e climate simulations improves the likeness to proxy data but it is clear that longer (3–4 ka) run times are required to fully test the consistency between models and data.

Plain Language Summary Investigating past warm periods can provide us with an analog for how climate will respond to future warming. In this study we compare the latest model simulations of Southern Ocean (SO) sea-surface temperatures and Antarctic winter sea-ice extent from 130,000 years ago with data from marine sediment cores. The simulations and sediment core data show the least match in the areas near the boundaries of the present day SO gyres (large, circulating ocean currents), implying that possibly changes in the position and size of the gyres are not fully recreated in the computer simulations. The inclusion of ice sheet meltwater into the North Atlantic improves the comparison between the simulations and sediment core data but it is clear that longer run times are required to fully test their consistency.

1. Introduction

In the present day, Antarctic winter sea-ice (WSI) covers an area of $\sim 18 \times 10^6$ km² and forms a critical component of the global climate system (Maksym, 2019). Sea ice has a high albedo or “reflectivity” (Hall, 2004), and seasonal growth in sea ice influences the strength of Southern Ocean (SO) and global overturning circulation through the formation of dense Antarctic shelf and bottom waters (Abernathey et al., 2016; Rintoul, 2018). Rising atmospheric greenhouse gas concentrations are driving current global warming, with a predicted reduction of 24%–34% in the Antarctic winter sea-ice extent (WSIE) by 2100 (Meredith et al., 2019). Model simulations have been unable to faithfully replicate recent changes in Antarctic sea ice unless they use unrealistically reduced warming trends (Rosenblum & Eisenman, 2017). This is likely due to the short length of the observational record and the complex climate dynamics and feedbacks associated with changes to modern WSIE (Hobbs et al., 2016; Purich et al., 2016). Marine Isotope Stage (MIS) 5e proxy records offer valuable evidence of a “warmer-than-present” climate, and the opportunity to improve our understanding/prediction of the impacts of future climate change.

During MIS 5e (130–116 ka) both mean annual global atmospheric temperatures and mean annual SO sea-surface temperatures (SSTs) peaked at $\sim 2^\circ\text{C}$ warmer than preindustrial (PI) (Capron et al., 2017; Fischer et al., 2018). A recent study has shown that, during MIS 5e, global sea levels were likely 1.2–5.3 m higher than the present day (Dyer et al., 2021). Unlike future anthropogenic warming, MIS 5e warming is forced by orbital changes, alongside a variety of internal ocean-ice-atmosphere feedbacks, rather than being driven by increasing atmospheric greenhouse gas concentrations. However, MIS 5e represents an important “laboratory” to evaluate climate model performance under warmer-than-present conditions.

Software: M.-V. Guarino
Supervision: L. C. Sime, C. S. Allen, M.-V. Guarino
Visualization: M. Chadwick
Writing – original draft: M. Chadwick
Writing – review & editing: L. C. Sime, C. S. Allen, M.-V. Guarino

Model simulations of the Peak MIS 5e climate at 127 ka are a part of the Coupled Model Intercomparison Project (CMIP6) and Paleoclimate Modelling Intercomparison Project (PMIP4) (Otto-Bliesner et al., 2017). Analysis of the short (50–100 years) orbitally forced CMIP6-PMIP4 ensembles indicates that these simulations exhibit SO summer SSTs_{model} (SSSTs) which were ~0.5°C cooler during Peak MIS 5e than the PI and that there was an average reduction of ~5%–8% in WSIE at 127 ka relative to the PI (Otto-Bliesner et al., 2021). These simulation results are a poor match for published Peak MIS 5e proxy records from SO marine sediment cores, which indicate a SSST_{proxy} warming of 0–5°C relative to the PI (Capron et al., 2017; Otto-Bliesner et al., 2021). The SO model-data discrepancy is hypothesized to be due to the absence of the Heinrich 11 (H11) meltwater event in CMIP6-PMIP4 Tier 1 simulations (Otto-Bliesner et al., 2021). Though we also note that model-data comparisons of MIS 5e Antarctic WSIE have been limited by the location of most published marine sediment core records: they are located north of the modern WSIE, and likely also north of the 127 ka WSIE (Chadwick et al., 2020; Holloway et al., 2017). The location of proxy records further restricts the ability to reconstruct summer sea-ice extent, with all MIS 5e marine sediment core records located north of the modern summer sea-ice edge (Chadwick et al., 2020, 2022b).

The inclusion of the H11 meltwater event in the North Atlantic in the latest model runs results in a slow-down in the Atlantic Meridional Overturning Circulation (AMOC), with a weakening of ~60% compared to non-meltwater-hosed runs (Guarino et al., 2023). Under a weakened AMOC, less heat is transported northwards, and the inclusion of H11 meltwater forcing is therefore expected to cause an additional increase in SO temperatures (Capron et al., 2017) and reduction in sea-ice cover (Holloway et al., 2018) relative to standard MIS 5e simulations, thus improving the match between models and proxy data.

The published syntheses of proxy records from SO marine sediment cores in Capron et al. (2017) and Chadwick et al. (2020) indicate Peak MIS 5e SSSTs_{proxy} were between 0 and 5°C warmer than the present and PI, with this warming anomaly decreasing toward the South Pole. The most southerly marine cores in these syntheses have SSST_{proxy} anomalies for Peak MIS 5e of <1.5°C (40°W–40°E), but there are no MIS 5e marine records located south of the modern Antarctic Polar Front (APF) for most of the SO (80°E–40°W).

Whilst most proxy records of Antarctic sea ice are located too far north to precisely constrain the Peak MIS 5e WSIE_{proxy}, a recent reconstruction suggests that the WSI edge was located 1–2° south of its modern position in the Pacific sector and >5° south of its modern position in the Atlantic sector (Chadwick et al., 2022b).

This study presents a new model-data comparison for the SO during MIS 5e. Peak MIS 5e Antarctic September sea-ice concentrations (SIC_{model}) and SO SSSTs_{model} from the latest UK fully-coupled HadGEM3-GC3.1 (hereafter HadGEM3) numerical simulations, both with and without the H11 meltwater event (Guarino et al., 2023), and from the H11 meltwater-hosed HadCM3 numerical simulations in Holloway et al. (2018) are compared with the latest diatom transfer function estimates of September SIC_{proxy} and SSSTs_{proxy} from nine marine sediment cores (Chadwick et al., 2021, 2022b) to answer the following:

Can we now tell if different areas of the SO show more or less consistency between model simulations and proxy data during MIS 5e?

Is H11 meltwater forcing necessary for the models to match the proxy records?

Are our current state of the art models capable of simulating the proxy data?

2. Materials and Methods

2.1. Numerical Simulations

HadGEM3 is a global coupled atmosphere-land-ocean-ice model which combines the Unified Model Atmosphere model (Walters et al., 2017), the JULES land surface model (Walters et al., 2017), the NEMO ocean model (Madec et al., 2019) and the CICE sea-ice model (J. K. Ridley et al., 2018). The atmosphere model has a horizontal resolution of 135 km and 85 vertical levels, and the ocean model has a horizontal resolution of 1° and 75 vertical levels. The PI control run is presented in Menary et al. (2018), uses a 700 years spin-up followed by a 200 years run length, and constant 1850 climate forcing (see Menary et al. (2018) for further details).

The standard Peak MIS 5e simulation (hereafter referred to as LIG_{HG}) is published in Guarino, Sime, Schröder, Malmierca-Vallet, et al. (2020) and the H11 simulation is published in Guarino et al. (2023). They were run using the protocol described in Otto-Bliesner et al. (2017) for Tier 1 and Tier 2 PMIP4 simulations. The Peak MIS 5e

climate was simulated by forcing the HadGEM3 model with constant last interglacial orbital and greenhouse gas boundary conditions (see Guarino et al. (2023) for further details), with all other boundary conditions consistent with the PI simulation (Menary et al., 2018). In the H11 run, the H11 meltwater event is simulated by adding a constant freshwater flux equal to 0.2 Sv, evenly across the North Atlantic between 50 and 70°N (Otto-Bliesner et al., 2017), with all other boundary conditions and forcings identical to the LIG_HG simulation (Guarino et al., 2023).

The LIG_HG simulation was spun-up for 350 years, to reach a quasi-atmospheric and upper-ocean equilibrium (Williams et al., 2020), followed by a production run of 200 years to account for model internal variability (Guarino, Sime, Schröder, Lister, et al., 2020). The H11 simulation was initialized from the end of the LIG_HG spin-up and run for 250 years. The climatological averages from the final 100 years (150–250 years), once the AMOC had reached a new equilibrium (Figure S1 in Supporting Information S1), are presented here (hereafter referred to as H11(250)_HG).

HadCM3 is a faster running, but older and lower resolution, UK model than HadGEM3, and is a coupled atmosphere-ocean general circulation model (Gordon et al., 2000) with the TRIFFID dynamic vegetation model (Cox, 2001) and MOSES 2.1 land surface model (Cox et al., 1998) included. The atmosphere model in HadCM3 has a horizontal resolution of 3.75° longitude by 2.5° latitude and 19 vertical levels, and the ocean model has a horizontal resolution of 1.25° and 20 vertical levels (Guarino, Sime, Schröder, Malmierca-Vallet, et al., 2020). HadCM3 has more simplified physics for the atmosphere, ocean, and sea ice than HadGEM3. The sea-ice scheme for HadCM3 uses a zero-layer thermodynamic model (Semtner, 1976), no sea-ice rheology, and applies wind stress to the ocean beneath the sea ice, with the top layer ocean current used for advection (Bryan, 1969). Whereas, for HadGEM3 the sea-ice scheme uses four sea-ice layers and a snow layer for the thermodynamics (Bitz & Lipscomb, 1999), a prognostic melt pond model (Flocco et al., 2012), and a elastic-viscous-plastic rheology with a remapping algorithm scheme for transport and advection (Hunke et al., 2015).

The HadCM3 simulations are published in Holloway et al. (2018), with 0.25 Sv freshwater forcing to the North Atlantic applied for 1600 years. We use the climatological averages for years 150–250 of the model run (hereafter referred to as H11(250)_HC), to match the length of the run performed for HadGEM3, and the last 100 years (1500–1600 years) (hereafter referred to as H11(1600)_HC), to examine how SSST_{model} and SIC_{model} evolved after a longer period of H11 type forcing.

MIS 5e SSST_{model} (average January to March (JFM)) are presented as anomalies relative to the PI control runs whereas September SIC_{model} are presented as absolute values.

2.2. Marine Sediment Cores

Modern Analog Technique (MAT) diatom transfer function estimates of September SIC_{proxy} and SSST_{proxy} for Peak MIS 5e, reconstructed from nine marine sediment cores and published in Chadwick et al. (2022b), are compared to model output. The transfer function methodology is detailed in Chadwick et al. (2022b) and the data for all the cores is available from Chadwick et al. (2021). In brief, the MAT transfer function compares the MIS 5e diatom species assemblages with a reference data set of 257 surface sediment samples. The five most similar surface sediment samples to each MIS 5e sample were identified using the chord distance and a weighted average of the environmental conditions for those five reference samples was used to reconstruct the conditions during MIS 5e. The reconstructed September SIC_{proxy} have a Root Mean Square Error of Prediction (RMSEP) of 0.09 and SSST_{proxy} have a RMSEP of 1.1°C. For PI SSST_{proxy} at each core site the average January-March SST_{proxy} from 1870 to 1900 was calculated from the HadISST1 data set (Rayner et al., 2003). The average SSST_{proxy} and September SIC_{proxy} in the 130–128 ka interval is considered to represent Peak MIS 5e conditions. This time interval is chosen as it is within the chronological uncertainty (± 2 ka) of both the peak $\delta^{18}\text{O}$ in the EPICA Dome C ice core record at ~ 128 ka (Sime et al., 2009) and the termination of the H11 meltwater event at 130 ka (Marino et al., 2015).

3. Results

3.1. SSST_{model} Anomalies

In both the LIG_HG and H11(250)_HG simulations the pattern of SSST_{model} anomalies for Peak MIS 5e relative to the PI is very similar (Figures 1a and 1b). Both runs show a cooling (0–1°C) in the Atlantic sector

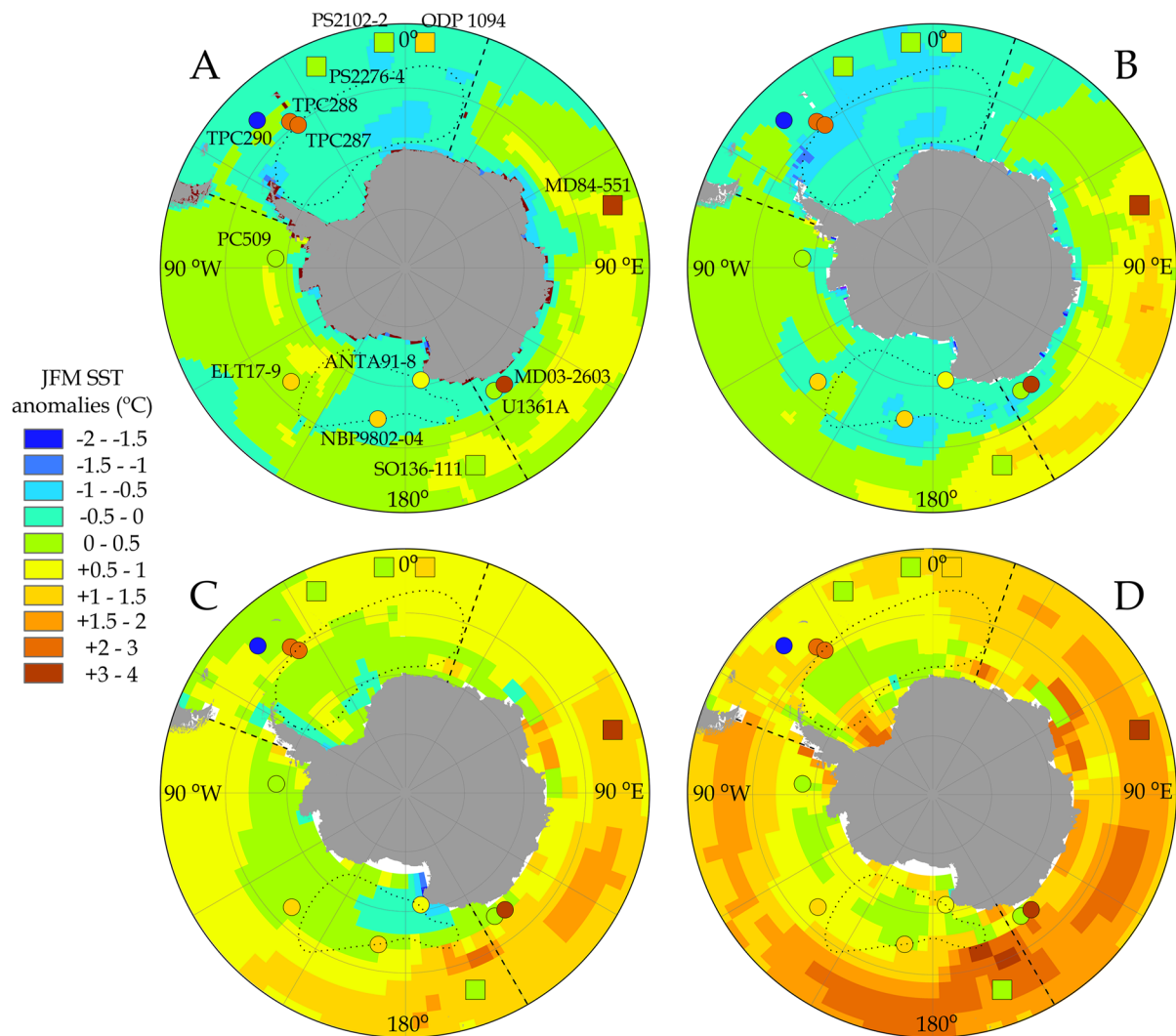


Figure 1. Maps of summer (January to March (JFM)) SST_{model} anomalies for Peak Marine Isotope Stage 5e relative to the preindustrial. (a) LIG_HG. (b) H11(250)_HG. (c) H11(250)_HC. (d) H11(1600)_HC. Colored circles on all maps represent the JFM SST_{proxy} anomalies from Chadwick et al. (2022b) and colored squares represent the SSST_{proxy} anomalies from Capron et al. (2017). The dashed black lines mark the boundaries between the three Southern Ocean sectors and the dotted black lines mark the modern extents of the Weddell Sea and Ross Sea gyres (positions of the Weddell Sea gyre is from Vernet et al. (2019) and the Ross Sea gyre is from Dotto et al. (2018)).

(70°W–20°E) and a warming (0–1.5°C) in the Indian sector (20–150°E) during Peak MIS 5e relative to the PI, with both trends more pronounced in the H11(250)_HG run (Figure 1b). In the Pacific sector (150°E–70°W), both the LIG_HG and H11(250)_HG simulations show a warming (0–1°C) in the eastern region (120–70°W) and a cooling (0–0.5°C) in the western region, south of the modern WSIE (150°E–150°W) but have diverging trends in the central area (150–120°W) where the LIG_HG run has a warming of up to 1°C and the H11(250)_HG run has a mixture of warming and cooling, all by less than 0.5°C (Figures 1a and 1b).

The H11(250)_HC and H11(1600)_HC simulations both have greater warming trends than either of the HadGEM3 runs, with only a few localized areas of cooling in the H11(250)_HC run and none in H11(1600)_HC run (Figures 1c and 1d). In the H11(250)_HC run, the area north of the modern WSIE had largely warmed by 0.5–1.5°C, whereas the region within the modern WSIE was generally less than 0.5°C warmer than PI (Figure 1c). In the H11(1600)_HC run the SSST_{model} anomalies have increased throughout the SO relative to the H11(250)_HC run, with the region within the modern WSIE mainly 0.5–1.5°C warmer than PI and the area to the north of the modern WSIE largely showing 1–3°C warming (Figure 1d). All simulations show the greatest Peak MIS 5e warming in the 90–170°E region, north of 60°S (Figure 1).

3.2. SSST_{proxy} Anomalies

With the exception of core TPC290, the sediment cores all indicate warmer conditions during Peak MIS 5e than the PI (Table 1 and Figure 1). The Pacific sector cores have SSST_{proxy} anomalies of less than 1.5°C, with the more southerly cores showing a warming of less than 1°C (Table 1). The nearby cores TPC288 and TPC287 in the Atlantic sector have similar SSST_{proxy} anomalies to each other, whereas, in the Indian sector, the proximally located cores MD03-2603 and U1361A have very different SSST_{proxy} anomalies to each other, with the SSST_{proxy} anomaly for core MD03-2603 more than 3°C warmer than the anomaly in core U1361A (Table 1 and Figure 1).

Within the $\pm 1.1^\circ\text{C}$ uncertainty on the diatom transfer function SSST_{proxy} values and the standard deviation of the model output, the Peak MIS 5e–PI SSST_{proxy} anomalies in all Pacific sector cores match the H11(250)_HC and H11(1600)_HC runs (Table 1 and Figures 1c and 1d). Proxy data for cores PC509 and ANTA91-8 also match the HadGEM3 model outputs (Table 1) and the proxy data in core ELT17-9 matches the LIG_HG run (Table 1). The transfer function Peak MIS 5e SSST_{proxy} anomaly in core U1361A also matches, within uncertainty, the values from all four model runs (Table 1). The transfer function SSST_{proxy} anomalies in cores TPC288 and MD03-2603 only match the model output for H11(1600)_HC and in core TPC287 there is not a match with any of the model outputs considered here (Table 1). Cores TPC288, TPC287, and MD03-2603 have SSST_{proxy} anomalies $>2^\circ\text{C}$ warmer than all the models and core TPC290 $> 1.5^\circ\text{C}$ cooler than all the models (Table 1).

3.3. September SICs_{model}

The patterns of September SICs_{model} are very similar between the HadGEM3 simulations (Figures 2a and 2b), with the main difference a greater WSIE_{model} in the H11(250)_HG run in the Pacific sector region 150–120°W and in the Weddell Sea to the east of the Antarctic Peninsula (Figure 2b). The HadCM3 simulations both have a reduced WSIE_{model} compared to the HadGEM3 runs, most notably in the eastern Weddell Sea (30°W–30°E) where the WSI edge is $>5^\circ$ latitude further south than either of the HadGEM3 runs (Figures 2c and 2d). In the H11(1600)_HC run, the September SICs_{model} are reduced compared to H11(250)_HC run, with the WSI edge 2–5° latitude further poleward in the former (Figure 2d).

3.4. September SICs_{proxy}

Within the ± 0.09 uncertainty on the transfer function September SIC_{proxy} values and two standard deviations of the model outputs, the Peak MIS 5e September SICs_{proxy} for many of the cores (TPC290, MD03-2603, U1361A and ANTA91-8) do not match any of the model runs (Table 1 and Figure 2). The match between model and proxy September SICs in the other cores is largely due to the high standard deviations of the model output. The proxy data in cores TPC288, TPC287, ELT17-9, and PC509 are the closest match for the H11(1600)_HC simulation (Table 1). The pattern of September SICs_{model} in the H11(1600)_HC simulation is also the best match with the transfer function values in the sediment cores (Figure 2d), with the greatest discrepancy evident in the expansion of western Pacific sector (150°E–150°W) WSIE_{model}, relative to the modern, in the H11(1600)_HC run, compared with the WSIE_{proxy} reduction evident in the sediment core data (Figure 2d).

4. Discussion

4.1. SSST_{model/proxy} Anomalies

For the Pacific sector core sites, the best model-data match for SSST_{model/proxy} anomalies is with the H11(1600)_HC run (Table 1 and Figure 1d), suggesting that the region south of 60°S in this sector was largely 0.5–1°C warmer than PI during Peak MIS 5e (Figure 1d). This SSST_{model} anomaly is consistent with the more southerly SO core sites in Capron et al. (2017) and Chadwick et al. (2020) and suggests that the region south of the APF warmed less than the rest of the SO during MIS 5e. The better match between the proxy data and the H11(1600)_HC simulation than between the proxy data and the H11(250)_HC simulation supports the need to run meltwater-hosed simulations for a longer duration than the 250 years in both the H11(250)_HG and H11(250)_HC runs.

In the Indian sector, all the model runs in this study indicate warmer conditions at core site MD03-2603 than the nearby U1361A (Table 1), but none of them have a difference of more than 0.8°C, whereas the transfer function SSST_{proxy} anomalies are $>3^\circ\text{C}$ warmer at core site MD03-2603 than U1361A (Table 1). The colder conditions around core U1361A could be due to increased melting of the Wilkes subglacial basin during MIS 5e (Wilson

Table 1
Diatom Transfer Function Values and Model Output for Peak Marine Isotope Stage (MIS) 5e September SICs_{model/proxy} and SSST_{model/proxy} Anomalies (Peak MIS 5e–preindustrial) for Nine Marine Sediment Core Locations and an Average for the Southern Ocean (SO) From the Model/Proxy Values at the Nine Core Sites

	TPC290	TPC288	TPC287	ELT17-9	NBP9802-04	MD03-2603	U1361A	PC509	ANTA91-8	SO average (mean ± st. dev.)
Latitude (°S), Longitude (°E)	55.55, -45.02	59.14, -37.96	60.31, -36.65	63.08, -135.12	64.20, -170.08	64.28, 139.38	64.41, 143.89	68.31, -86.03	70.78, 172.83	–
SSST _{proxy} anomaly (°C)	-1.70 ± 1.10	+2.65 ± 1.10	+2.75 ± 1.10	+1.24 ± 1.10	+1.43 ± 1.10	+3.13 ± 1.10	+0.04 ± 1.10	+0.24 ± 1.10	+1.00 ± 1.10	+1.56 ± 1.19
LIG_HG SSST _{model} anomaly (°C)	-0.03 ± 0.67	-0.19 ± 0.90	-0.31 ± 1.02	+0.19 ± 0.91	-0.32 ± 1.06	-0.19 ± 1.05	-0.20 ± 1.18	+0.25 ± 1.01	-0.10 ± 0.29	-0.10 ± 0.04
H11(250)_HG SSST _{model} anomaly (°C)	-0.16 ± 0.60	-0.50 ± 0.90	-0.78 ± 0.92	-0.03 ± 1.11	-0.55 ± 1.00	-0.50 ± 1.07	-0.66 ± 1.17	-0.02 ± 0.83	-0.13 ± 0.26	-0.37 ± 0.07
H11(250)_HC SSST _{model} anomaly (°C)	+0.45 ± 0.72	+0.67 ± 0.82	+0.62 ± 0.81	+0.23 ± 0.61	+0.17 ± 0.60	+0.62 ± 0.89	+0.41 ± 0.74	+0.05 ± 0.52	-0.04 ± 0.74	+0.35 ± 0.06
H11(1600)_HC SSST _{model} anomaly (°C)	+0.94 ± 0.72	+1.11 ± 0.92	+0.49 ± 0.84	+0.77 ± 0.63	+0.55 ± 0.66	+1.34 ± 0.84	+0.73 ± 1.00	+0.45 ± 0.54	+0.39 ± 0.73	+0.75 ± 0.09
September SIC _{proxy}	0.19 ± 0.09	0.23 ± 0.09	0.22 ± 0.09	0.13 ± 0.09	0.11 ± 0.09	0.19 ± 0.09	0.63 ± 0.09	0.34 ± 0.09	0.62 ± 0.09	0.30 ± 0.03
LIG_HGSeptember SIC _{model}	0.00 ± 0.00	0.71 ± 0.62	0.89 ± 0.32	0.00 ± 0.00	0.67 ± 0.58	0.93 ± 0.12	0.93 ± 0.08	0.73 ± 0.58	0.96 ± 0.02	0.65 ± 0.13
H11(250)_HG September SIC _{model}	0.00 ± 0.00	0.79 ± 0.44	0.94 ± 0.10	0.01 ± 0.06	0.80 ± 0.42	0.94 ± 0.10	0.94 ± 0.06	0.85 ± 0.34	0.95 ± 0.02	0.69 ± 0.14
H11(250)_HC September SIC _{model}	0.00 ± 0.03	0.42 ± 0.28	0.42 ± 0.32	0.66 ± 0.32	0.96 ± 0.02	0.94 ± 0.13	0.95 ± 0.09	0.47 ± 0.36	0.97 ± 0.00	0.64 ± 0.10
H11(1600)_HC September SIC _{model}	0.00 ± 0.03	0.22 ± 0.25	0.22 ± 0.28	0.17 ± 0.35	0.94 ± 0.02	0.93 ± 0.13	0.94 ± 0.09	0.19 ± 0.33	0.97 ± 0.01	0.51 ± 0.16

Note. Diatom transfer function values for Peak MIS 5e are an average of the 130–128 ka interval and are presented in Chadwick et al. (2022b). For the model output, pink shading indicates conditions that are warmer/have less sea ice than the proxy values, blue shading indicates conditions that are colder/have more sea ice, and no shading indicates conditions that match the proxy values within uncertainty. The errors on the proxy data for each core are the RMSEP values for the diatom transfer function (Section 2.2) and the errors on the model data at each core site are two standard deviations for the September SICs and one standard deviation for the SSST anomalies (cf. Guarino, Sime, Schröder, Malmierca-Vallet, et al., 2020).

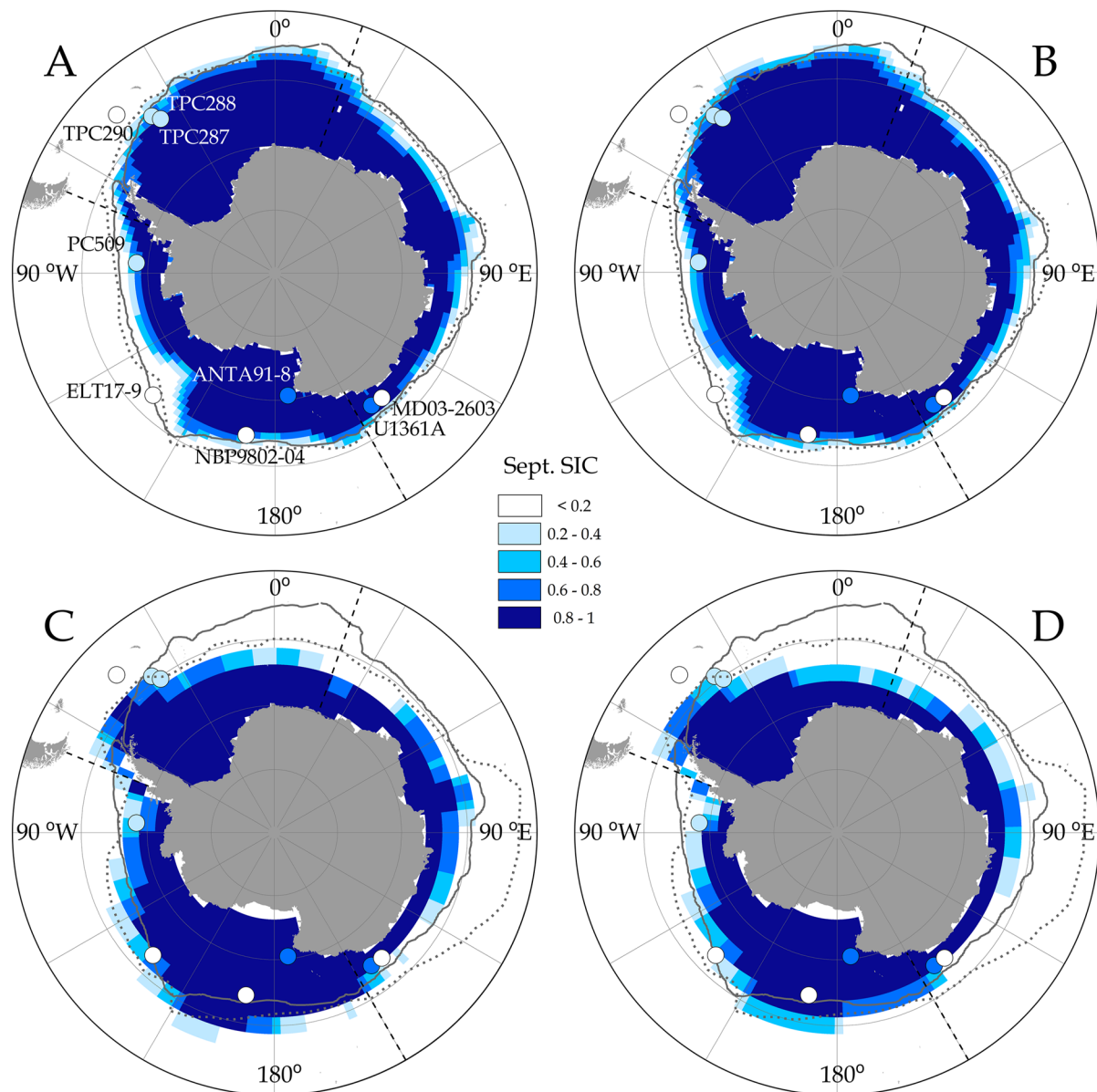


Figure 2. Maps of September SIC_{model} for Peak Marine Isotope Stage 5e. (a) LIG_HG. (b) H11(250)_HG. (c) H11(250)_HC. (d) H11(1600)_HC. Colored circles on all maps represent the September SIC_{proxy} in Chadwick et al. (2022b). The solid gray line on all maps marks the modern (1981–2010) median September sea-ice extent (Fetterer et al., 2017), the dotted gray lines mark the September sea-ice extent from the preindustrial (PI) model runs (HadCM3 PI extent is from Turner et al., 2001), and the dashed black lines mark the boundaries between the three Southern Ocean sectors.

et al., 2018). The shelf bathymetry would likely funnel any colder glacial meltwaters toward U1361A rather than MD03-2603 (Behrens et al., 2019), promoting the difference in $SSST_{model/proxy}$ anomalies. However, this does not explain why the $SSST_{proxy}$ anomaly for core MD03-2603 is still $>2^{\circ}C$ greater than any of the model results.

The colder-than-PI $SSST_{proxy}$ in core TPC290 is anomalous when compared to the nearby Atlantic sector cores TPC288 and TPC287 (Figure 1 and Table 1). This is likely a result of high abundances of the diatom group *Chaetoceros* resting spores (rs.) during MIS 5e (Chadwick & Allen, 2021), as discussed in Chadwick et al. (2022b). This diatom group is associated with meltwater stratification (Crosta et al., 1997) and WSI (Armand et al., 2005) and is found in highest present day abundances along the Antarctic Peninsula. Therefore, the high *Chaetoceros* rs. abundances in core TPC290 MIS 5e samples are likely to be misattributed to the colder conditions along the Antarctic Peninsula than to the Scotia Sea, where there are no modern samples in the transfer function reference data set (Chadwick et al., 2022b).

None of the model runs considered here are able to recreate the $\sim 2.7^{\circ}\text{C}$ $\text{SSST}_{\text{proxy}}$ anomaly in the Atlantic sector cores TPC288 and TPC287 (Table 1 and Figure 1). This discrepancy could be as a result of a poleward constriction of the northern limb of the Weddell Gyre not materializing in the model runs. A constriction of the Weddell Gyre would displace warm ($>1.5^{\circ}\text{C}$) surface waters to the south during Peak MIS 5e, causing larger positive $\text{SSST}_{\text{proxy}}$ anomalies at cores TPC288 and TPC287 than if both cores had remained bathed by Weddell Sea surface waters during Peak MIS 5e. A reduction in the extent of the Weddell Gyre during MIS 5e is supported by the findings of Ghadi et al. (2020) and Chadwick et al. (2022a) and is consistent with the increased strength of the Antarctic Circumpolar Current during MIS 5e relative to the recent shown by Wu et al. (2021).

A CMIP3 and CMIP5 model ensemble by Wang (2013) identified that subpolar gyre areal extent displays a diverse response to warmer-than-present climatic conditions, with trends varying from a $23 \times 10^{10} \text{ m}^2/\text{decade}$ decrease to a $69 \times 10^{10} \text{ m}^2/\text{decade}$ increase between models. The HadCM3 run included in this ensemble showed a slight increasing trend in areal extent of $1 \times 10^{10} \text{ m}^2/\text{decade}$ and the barotropic stream functions from the LIG_HG and H11(250)_HG simulations (Figure S2 in Supporting Information S1) indicate that the model position of the Weddell and Ross Sea gyres is very similar to their modern positions. This all supports minimal, or no, poleward contraction in model gyre positions during MIS 5e, relative to today, in contrast to the hypothesized contraction evidenced by the proxy records. Our proxy-model comparison could therefore be highlighting deficiencies in subpolar gyre evolution in models, with the greatest model-data discrepancies from the core sites at the edges of the present-day gyre extents.

Both Kuhlbrodt et al. (2018) and Menary et al. (2018) indicate that SO circulation in HadGEM3 simulations of the PI and present day show a fairly close match to observations. Therefore the discrepancy between $\text{SSST}_{\text{proxy}}$ anomalies and $\text{SSST}_{\text{model}}$ anomalies is not just an artifact of the model being unable to faithfully recreate PI circulation in the SO.

It is also possible that the discrepancy between $\text{SSST}_{\text{proxy}}$ anomalies and $\text{SSST}_{\text{model}}$ anomalies for cores TPC288 and TPC287 is as a result of the simulations not being run for a sufficient duration for the meltwater-induced warming perturbation to fully propagate across the SO. The improved match between $\text{SSST}_{\text{proxy}}$ anomalies and $\text{SSST}_{\text{model}}$ anomalies for the H11(1600)_HC simulation than for the H11(250)_HC simulation (Figure 1) suggests that running meltwater forced simulations for a longer duration could result in $\text{SSST}_{\text{model}}$ anomalies consistent with the $\text{SSST}_{\text{proxy}}$ anomalies in cores TPC288 and TPC287.

The $>2^{\circ}\text{C}$ $\text{SSST}_{\text{proxy}}$ anomalies in cores TPC288, TPC287, and MD03-2603 are greater than other published $\text{SSST}_{\text{proxy}}$ anomalies from the region south of the APF (Capron et al., 2017; Chadwick et al., 2020) and contrasts with the pattern of decreased $\text{SSST}_{\text{proxy}}$ anomalies toward the continent. The largest $\text{SSST}_{\text{proxy}}$ anomalies in the Capron et al. (2017) and Chadwick et al. (2020) syntheses were found in cores that were likely bathed by different surface water masses during MIS 5e compared to present/PI (Chadwick et al., 2020), indicating that this is likely also the case for core sites TPC288, TPC287, and MD03-2603. This difference in the surface water mass above the core sites could have been caused by either changes in gyre extent, in the case of cores TPC288 and TPC287, or by movement of Antarctic Circumpolar Current fronts, in the case of core MD03-2603 (Chadwick et al., 2022b). Comparing the $\text{SSST}_{\text{proxy}}$ anomalies in the Atlantic and Indian sectors with the Pacific sector shows that there is strong longitudinal heterogeneity in $\text{SSST}_{\text{proxy}}$ anomalies in addition to the latitudinal variation identified by Chadwick et al. (2020).

For the SO south of the APF, Capron et al. (2017) reconstructed a mean $\text{SSST}_{\text{proxy}}$ anomaly of $+1.4 \pm 1.2^{\circ}\text{C}$ during Peak MIS 5e relative to the PI and Chadwick et al. (2022b) reconstructed a mean $\text{SSST}_{\text{proxy}}$ anomaly of $+1.6 \pm 1.2^{\circ}\text{C}$ relative to the PI. Combining these syntheses indicates that the SO south of the APF averaged $1.5 \pm 1.2^{\circ}\text{C}$ warmer during Peak MIS 5e than the PI.

4.2. September SICs_{model/proxy}

In the western Pacific (Ross Sea) sector all the model runs appear to overestimate Peak MIS 5e WSIE_{model}, with the HadCM3 runs even indicating an expansion in WSIE_{model} relative to the modern (Figures 2c and 2d). The eastern Pacific sector has better model-data agreement, especially for the H11(250)_HG and H11(1600)_HC runs (Figures 2b and 2d). The shape of modern Pacific sector WSIE is strongly influenced by the position of the APF and the shape and position of the Ross Sea Gyre (Nghiem et al., 2016), with the proxy data indicating a poleward movement of the APF and contraction of the Ross Sea Gyre in the western Pacific sector which is less apparent in the models.

A similar poleward contraction of the Weddell Gyre during MIS 5e, as previously hypothesized with the $SSST_{proxy}$ anomalies in cores TPC288 and TPC287 (Section 4.1), would also help explain the shape of the $WSIE_{model}$ in the HadCM3 runs (Figures 2c and 2d), with a longitudinal constriction of the Weddell Gyre during MIS 5e also supported by proxy data from the western Indian sector (Ghadi et al., 2020). Alternatively, running meltwater forced simulations for a longer duration could also result in an improved match between $SICs_{proxy}$ and $SICs_{model}$ for cores TPC288 and TPC287, with an improved model-proxy match already seen in H11(1600)_HC compared to H11(250)_HC (Figure 2).

The shape of the eastern Indian sector $WSIE_{model}$ in the HadCM3 simulations in the proximity of cores MD03-2603 and U1361A (Figures 2c and 2d) is consistent with the greater Peak MIS 5e September SIC_{proxy} reconstructed for core U1361A. High glacial meltwater flux can promote increased $WSIE$ (Merino et al., 2018) and the configuration of the eastern Indian sector $WSIE$ therefore supports a large release of glacial meltwater from the Wilkes subglacial basin during MIS 5e (Wilson et al., 2018), which was channeled toward core U1361A rather than core MD03-2603, as discussed in Section 4.1. Many of the estimates of Peak MIS 5e September SIC_{proxy} have a good visual similarity to the models (Figure 2) but do not match the models within the transfer function uncertainty (Table 1). This discrepancy is due to the steep gradient in SIC fraction, with values between 0.2 and 0.8 occupying only a small geographic area (Figure 2), and therefore small variations in the position of the WSI edge can make a large difference to the Peak MIS 5e September $SIC_{model/proxy}$ at most of the core sites. This is supported by the high standard deviation of model output for September $SICs_{model}$ between 0.2 and 0.8 (Table 1).

5. Conclusions

Reconstructed Peak MIS 5e September $SICs_{proxy}$ and $SSST_{proxy}$ anomalies display variation both within and between SO sectors (Figures 1 and 2). The greatest discrepancies between the proxy data and the simulation results are for the $WSIE$ in the western Pacific sector and the $SSSTs$ in the Atlantic sector (Figures 1 and 2), which could be due to a poleward contraction of the Ross Sea and Weddell Gyres, respectively, that is not fully realized in the models, or could also be as a result of the meltwater hosed simulations not having been run for a sufficient duration.

Of the four HadGEM3 and HadCM3 simulations presented in this study, the best match to the proxy data is provided by the H11(1600)_HC simulation (Figures 1d and 2d and Table 1). The better model-data agreement for the H11(1600)_HC run than for the H11(250)_HC run supports the importance of including North Atlantic meltwater hosing in models of Peak MIS 5e climate and running the models for longer than 250 years. The importance of this meltwater hosing in MIS 5e reconstructions has also been shown through transient modeling of Termination II in Obase et al. (2021). The short run length of the H11(250)_HG simulation explains the poor match to the proxy data as the output is more likely reflective of the conditions at ~133 ka (Holloway et al., 2018; Marino et al., 2015) than 130–128 ka. Guarino et al. (2023) showed that after 250 years of meltwater hosing, the global heat transport south of 55°S remained unaffected in HadGEM3 simulations, which would explain why the $WSIE$ in H11(250)_HG does not show any more consistency with the proxy records than the non-meltwater forced LIG_HG simulation.

Running the meltwater hosed H11(250)_HG simulation for a longer duration, ideally 3–4 ka (Marino et al., 2015), is crucial for investigating how well the latest simulations match with the Peak MIS 5e conditions reconstructed from marine sediment cores. Whilst the existing evidence suggests that H11 meltwater forcing is required to get a match between the models and proxy data, the current model run-duration is too short and likely needs to be run for at least 1500 years for us to know whether state of the art models are capable of matching the Peak MIS 5e conditions evidenced by the proxy data. Of particular interest in the analysis of longer HadGEM3 runs would be to assess whether the model would resolve the greater reduction in the Atlantic sector $WSIE_{model/proxy}$ seen in both sediment core data (Chadwick et al., 2022a, 2022b) and previous models (Holloway et al., 2017; Holloway et al., 2018) but absent from either the LIG_HG or H11(250)_HG simulations (Figures 2a and 2b). Additionally, for future model runs there potentially needs to be additional focus on how the Weddell Sea and Ross Sea gyres are realized in the simulations.

Conflict of Interest

The authors declare no conflicts of interest relevant to this study.

Data Availability Statement

The MIS 5e September SIC and SSST data for the nine marine sediment cores, produced using the Modern Analog Technique, are available from PANGAEA (Chadwick et al., 2021). All HadGEM3 and HadCM3 model output presented in this manuscript are available as netCDF files from Mendeley (Chadwick & Guarino, 2023). Additionally the PI HadGEM3 output is available from the Earth System Grid Federation (J. Ridley et al., 2018).

Acknowledgments

The Natural Environmental Research Council (Grant NE/L002531/1) supported this work. LCS and MVG acknowledge the financial support of National Environmental Research Council research Grants NE/P013279/1 and NE/P009271/1, respectively. This project has received funding from the European Union's Horizon 2020 research and innovation programme under Grant agreement No. 820970. This research also contributes to the British Antarctic Survey's "Polar Science for Planet Earth" programme. Our thanks to both Sentia Goursaud, Irene Malmierca Vallet, and Rahul Sivankutty for assisting in both accessing and formatting the HadCM3 output data from Holloway et al. (2018). This work used the ARCHER UK National Supercomputing Service (<http://www.archer.ac.uk>) and the JASMIN analysis platform (<https://www.ceda.ac.uk/services/jasmin/>).

References

- Abernathy, R. P., Ceroveckı, I., Holland, P. R., Newsom, E., Mazloff, M., & Talley, L. D. (2016). Water-mass transformation by sea ice in the upper branch of the Southern Ocean overturning. *Nature Geoscience*, 9(8), 596–601. <https://doi.org/10.1038/ngeo2749>
- Armand, L. K., Crosta, X., Romero, O., & Pichon, J.-J. (2005). The biogeography of major diatom taxa in Southern Ocean sediments: 1. Sea ice related species. *Palaeogeography, Palaeoclimatology, Palaeoecology*, 223(1–2), 93–126. <https://doi.org/10.1016/j.palaeo.2005.02.015>
- Behrens, B., Miyairi, Y., Sproson, A. D., Yamane, M., & Yokoyama, Y. (2019). Meltwater discharge during the Holocene from the Wilkes subglacial basin revealed by beryllium isotopes analysis of marine sediments. *Journal of Quaternary Science*, 34(8), 603–608. <https://doi.org/10.1002/jqs.3148>
- Bitz, C. M., & Lipscomb, W. H. (1999). An energy-conserving thermodynamic model of sea ice. *Journal of Geophysical Research*, 104(C7), 15669–15677. <https://doi.org/10.1029/1999jc900100>
- Bryan, K. (1969). Climate and the ocean circulation III. The ocean model. *Monthly Weather Review*, 97(11), 806–827. [https://doi.org/10.1175/1520-0493\(1969\)097<0806:catoc>2.3.co;2](https://doi.org/10.1175/1520-0493(1969)097<0806:catoc>2.3.co;2)
- Capron, E., Govin, A., Feng, R., Otto-Bliessner, B. L., & Wolff, E. W. (2017). Critical evaluation of climate syntheses to benchmark CMIP6/PMIP4 127 ka Last Interglacial simulations in the high-latitude regions. *Quaternary Science Reviews*, 168, 137–150. <https://doi.org/10.1016/j.quascirev.2017.04.019>
- Chadwick, M., & Allen, C. S. (2021). Marine Isotope Stage 5e diatom assemblages in marine sediment core TPC290 (–55.55°N, –45.02°E, Cruise JR48) [Dataset]. UK Polar Data Centre, Natural Environment Research Council, UK Research & Innovation. <https://doi.org/10.5285/D7C00BEA-659A-426E-942F-821F6517C449>
- Chadwick, M., Allen, C. S., & Crosta, X. (2021). MIS 5e Southern Ocean September sea-ice concentrations and summer sea-surface temperatures reconstructed from marine sediment cores using a MAT diatom transfer function [Dataset]. PANGAEA. <https://doi.org/10.1594/PANGAEA.936573>
- Chadwick, M., Allen, C. S., Sime, L. C., Crosta, X., & Hillenbrand, C.-D. (2022a). How does the Southern Ocean palaeoenvironment during Marine Isotope Stage 5e compare to the modern? *Marine Micropaleontology*, 170, 102066. <https://doi.org/10.1016/j.marmicro.2021.102066>
- Chadwick, M., Allen, C. S., Sime, L. C., Crosta, X., & Hillenbrand, C.-D. (2022b). Reconstructing Antarctic winter sea-ice extent during Marine Isotope Stage 5e. *Climate of the Past*, 18(1), 129–146. <https://doi.org/10.5194/cp-18-129-2022>
- Chadwick, M., Allen, C. S., Sime, L. C., & Hillenbrand, C. D. (2020). Analysing the timing of peak warming and minimum winter sea-ice extent in the Southern Ocean during MIS 5e. *Quaternary Science Reviews*, 229, 106134. <https://doi.org/10.1016/j.quascirev.2019.106134>
- Chadwick, M., & Guarino, M.-V. (2023). MIS 5e September sea-ice concentrations and summer SST anomalies (relative to the preindustrial) from HadGEM3 and HadCM3 model simulations [Dataset]. Mendeley Data. <https://doi.org/10.17632/84v5y732hd.1>
- Cox, P., & Met Office. (2001). *Description of the "TRIFFID" dynamic global vegetation model* (Vol. 24). Hadley Centre Technical Note.
- Cox, P. M., Huntingford, C., & Harding, R. J. (1998). A canopy conductance and photosynthesis model for use in a GCM land surface scheme. *Journal of Hydrology*, 212–213, 79–94. [https://doi.org/10.1016/S0022-1694\(98\)00203-0](https://doi.org/10.1016/S0022-1694(98)00203-0)
- Crosta, X., Pichon, J.-J., & Labracherie, M. (1997). Distribution of *Chaetoceros* resting spores in modern peri-Antarctic sediments. *Marine Micropaleontology*, 29(3–4), 283–299. [https://doi.org/10.1016/S0377-8398\(96\)00033-3](https://doi.org/10.1016/S0377-8398(96)00033-3)
- Dotto, T. S., Naveira Garabato, A., Bacon, S., Tsamados, M., Holland, P. R., Hooley, J., et al. (2018). Variability of the Ross Gyre, Southern Ocean: Drivers and responses revealed by satellite altimetry. *Geophysical Research Letters*, 45, 6195–6204. <https://doi.org/10.1029/2018gl078607>
- Dyer, B., Austermann, J., D'Andrea, W. J., & Raymo, M. E. (2021). Sea-level trends across The Bahamas constrain peak last interglacial ice melt. *Proceedings of the National Academy of Sciences*, 118(33), e2026839118.
- Fetterer, F., Knowles, K., Meier, W. N., Savoie, M., & Windnagel, A. K. (2017). *Sea ice index, Version 3*. NSIDC: National Snow and Ice Data Center.
- Fischer, H., Meissner, K. J., Mix, A. C., Abram, N. J., Austermann, J., Brovkin, V., et al. (2018). Palaeoclimate constraints on the impact of 2°C anthropogenic warming and beyond. *Nature Geoscience*, 11(7), 474–485. <https://doi.org/10.1038/s41561-018-0146-0>
- Flocco, D., Schroeder, D., Feltham, D. L., & Hunke, E. C. (2012). Impact of melt ponds on Arctic sea ice simulations from 1990 to 2007. *Journal of Geophysical Research*, 117(C9), C09032. <https://doi.org/10.1029/2012jc008195>
- Ghadi, P., Nair, A., Crosta, X., Mohan, R., Manoj, M. C., & Meloth, T. (2020). Antarctic sea-ice and palaeoproductivity variation over the last 156,000 years in the Indian sector of Southern Ocean. *Marine Micropaleontology*, 160, 101894. <https://doi.org/10.1016/j.marmicro.2020.101894>
- Gordon, C., Cooper, C., Senior, C. A., Banks, H., Gregory, J. M., Johns, T. C., et al. (2000). The simulation of SST, sea ice extents and ocean heat transports in a version of the Hadley Centre coupled model without flux adjustments. *Climate Dynamics*, 16(2–3), 147–168. <https://doi.org/10.1007/s003820050010>
- Guarino, M.-V., Sime, L. C., Diamond, R., Ridley, J., & Schroeder, D. (2023). The coupled system response to a 250 years of freshwater forcing: Last Interglacial CMIP6-PMIP4 HadGEM3 simulations. *Climate of the Past*, 19(4), 865–881. <https://doi.org/10.5194/cp-19-865-2023>
- Guarino, M.-V., Sime, L. C., Schröder, D., Lister, G., & Hatcher, R. (2020). Machine dependence and reproducibility for coupled climate simulations: The HadGEM3-GC3.1 CMIP Preindustrial simulation. *Geoscientific Model Development*, 13(1), 139–154. <https://doi.org/10.5194/gmd-13-139-2020>
- Guarino, M.-V., Sime, L. C., Schröder, D., Malmierca-Vallet, I., Rosenblum, E., Ringer, M., et al. (2020). Sea-ice-free Arctic during the Last Interglacial supports fast future loss. *Nature Climate Change*, 10(10), 928–932. <https://doi.org/10.1038/s41558-020-0865-2>
- Hall, A. (2004). The role of surface albedo feedback in climate. *Journal of Climate*, 17(7), 1550–1568. [https://doi.org/10.1175/1520-0442\(2004\)017<1550:trosaf>2.0.co;2](https://doi.org/10.1175/1520-0442(2004)017<1550:trosaf>2.0.co;2)
- Hobbs, W. R., Massom, R., Stammerjohn, S., Reid, P., Williams, G., & Meier, W. (2016). A review of recent changes in Southern Ocean sea ice, their drivers and forcings. *Global and Planetary Change*, 143, 228–250. <https://doi.org/10.1016/j.gloplacha.2016.06.008>
- Holloway, M. D., Sime, L. C., Allen, C. S., Hillenbrand, C.-D., Bunch, P., Wolff, E., & Valdes, P. J. (2017). The spatial structure of the 128 ka Antarctic sea ice minimum. *Geophysical Research Letters*, 44(21), 11129–11139. <https://doi.org/10.1002/2017gl074594>

- Holloway, M. D., Sime, L. C., Singarayer, J. S., Tindall, J. C., & Valdes, P. J. (2018). Simulating the 128-ka Antarctic climate response to Northern Hemisphere ice sheet melting using the isotope-enabled HadCM3. *Geophysical Research Letters*, *45*(21), 11921–11929. <https://doi.org/10.1029/2018gl079647>
- Hunke, E., Lipscomb, W., Turner, A., Jeffery, N., & Elliott, S. (2015). *CICE: The Los Alamos sea ice model documentation and software user's manual version 5* (Tech. Rep. LA-CC-06-012). Los Alamos National Laboratory.
- Kuhlbrodt, T., Jones, C. G., Sellar, A., Storkey, D., Blockley, E., Stringer, M., et al. (2018). The low-resolution version of HadGEM3 GC3.1: Development and evaluation for global climate. *Journal of Advances in Modeling Earth Systems*, *10*(11), 2865–2688. <https://doi.org/10.1029/2018ms001370>
- Madec, G., Bourdalle-Badie, R., Chanut, J., Clementi, E., Coward, A., Ethe, C., et al. (2019). *NEMO ocean engine*. Notes Du Pole De Modelisation De L'institut Pierre-simon Laplace (IPSL).
- Maksym, T. (2019). Arctic and Antarctic Sea ice change: Contrasts, commonalities, and causes. *Annual Review of Marine Science*, *11*(1), 187–213. <https://doi.org/10.1146/annurev-marine-010816-060610>
- Marino, G., Rohling, E. J., Rodriguez-Sanz, L., Grant, K. M., Heslop, D., Roberts, A. P., et al. (2015). Bipolar seesaw control on last interglacial sea level. *Nature*, *522*(7555), 197–201. <https://doi.org/10.1038/nature14499>
- Menary, M. B., Kuhlbrodt, T., Ridley, J., Andrews, M. B., Dimdore-Miles, O. B., Deshayes, J., et al. (2018). Preindustrial control simulations with HadGEM3-GC3.1 for CMIP6. *Journal of Advances in Modeling Earth Systems*, *10*, 3049–3075. <https://doi.org/10.1029/2018ms001495>
- Meredith, M., Sommerkorn, M., Cassotta, S., Derksen, C., Ekaykin, A., Hollowed, A., et al. (2019). Polar regions. In H. O. Portner, D. C. Roberts, V. Masson-Delmotte, P. Zhai, M. Tignor, E. Poloczanska, et al. (Eds.), *IPCC special report on the ocean and cryosphere in a changing climate* (pp. 203–320). Cambridge University Press.
- Merino, N., Jourdain, N. C., Le Sommer, J., Goosse, H., Mathiot, P., & Durand, G. (2018). Impact of increasing Antarctic glacial freshwater release on regional sea-ice cover in the Southern Ocean. *Ocean Modelling*, *121*, 76–89. <https://doi.org/10.1016/j.ocemod.2017.11.009>
- Nghiem, S. V., Rigor, I. G., Clemente-Colón, P., Neumann, G., & Li, P. P. (2016). Geophysical constraints on the Antarctic sea ice cover. *Remote Sensing of Environment*, *181*, 281–292. <https://doi.org/10.1016/j.rse.2016.04.005>
- Obase, T., Abe-Ouchi, A., & Saito, F. (2021). Abrupt climate changes in the last two deglaciations simulated with different Northern ice sheet discharge and insolation. *Scientific Reports*, *11*(1), 22359. <https://doi.org/10.1038/s41598-021-01651-2>
- Otto-Bliensner, B. L., Braconnot, P., Harrison, S. P., Lunt, D. J., Abe-Ouchi, A., Albani, S., et al. (2017). The PMIP4 contribution to CMIP6—Part 2: Two interglacials, scientific objective and experimental design for Holocene and Last Interglacial simulations. *Geoscientific Model Development*, *10*(11), 3979–4003. <https://doi.org/10.5194/gmd-10-3979-2017>
- Otto-Bliensner, B. L., Brady, E. C., Zhao, A., Brierley, C., Axford, Y., Capron, E., et al. (2021). Large-scale features of Last Interglacial climate: Results from evaluating the *lig127k* simulations for the Coupled Model Intercomparison Project (CMIP6)-Paleoclimate Modeling Intercomparison Project (PMIP4). *Climate of the Past*, *17*(1), 63–94. <https://doi.org/10.5194/cp-17-63-2021>
- Purich, A., England, M. H., Cai, W., Chikamoto, Y., Timmermann, A., Fyfe, J. C., et al. (2016). Tropical Pacific SST drivers of recent Antarctic sea ice trends. *Journal of Climate*, *29*(24), 8931–8948. <https://doi.org/10.1175/jcli-d-16-0440.1>
- Rayner, N. A., Parker, D. E., Horton, E. B., Folland, C. K., Alexander, L. V., Rowell, D. P., et al. (2003). Global analyses of sea surface temperature, sea ice, and night marine air temperature since the late nineteenth century. *Journal of Geophysical Research*, *108*(D14), 4407. <https://doi.org/10.1029/2002jd002670>
- Ridley, J., Menary, M. B., Kuhlbrodt, T., Andrews, M. B., & Andrews, T. (2018). MOHC HadGEM3-GC31-LL model output prepared for CMIP6 CMIP [Dataset]. Earth System Grid Federation. <https://doi.org/10.22033/ESGF/CMIP6.419>
- Ridley, J. K., Blockley, E. W., Keen, A. B., Rae, J. G. L., West, A. E., & Schroeder, D. (2018). The sea ice model component of HadGEM3-GC3.1. *Geoscientific Model Development*, *11*(2), 713–723. <https://doi.org/10.5194/gmd-11-713-2018>
- Rintoul, S. R. (2018). The global influence of localized dynamics in the Southern Ocean. *Nature*, *558*(7709), 209–218. <https://doi.org/10.1038/s41586-018-0182-3>
- Rosenblum, E., & Eisenman, I. (2017). Sea ice trends in climate models only accurate in runs with biased global warming. *Journal of Climate*, *30*(16), 6265–6278. <https://doi.org/10.1175/jcli-d-16-0455.1>
- Semtner, A. J. (1976). A model for the thermodynamic growth of sea ice in numerical investigations of climate. *Journal of Physical Oceanography*, *6*(3), 379–389. [https://doi.org/10.1175/1520-0485\(1976\)006<0379:amftgt>2.0.co;2](https://doi.org/10.1175/1520-0485(1976)006<0379:amftgt>2.0.co;2)
- Sime, L. C., Wolff, E. W., Oliver, K. I., & Tindall, J. C. (2009). Evidence for warmer interglacials in East Antarctic ice cores. *Nature*, *462*(7271), 342–345. <https://doi.org/10.1038/nature08564>
- Turner, J., Connolley, W., Cresswell, D., & Harangozo, S. (2001). The simulation of Antarctic sea ice in the Hadley Centre Climate Model (HadCM3). *Annals of Glaciology*, *33*, 585–591. <https://doi.org/10.3189/172756401781818095>
- Vernet, M., Geibert, W., Hoppema, M., Brown, P. J., Haas, C., Hellmer, H. H., et al. (2019). The Weddell Gyre, Southern Ocean: Present knowledge and future challenges. *Reviews of Geophysics*, *57*(3), 623–708. <https://doi.org/10.1029/2018rg000604>
- Walters, D., Boutle, I., Brooks, M., Melvin, T., Stratton, R., Vosper, S., et al. (2017). The Met Office unified model global atmosphere 6.0/6.1 and JULES global land 6.0/6.1 configurations. *Geoscientific Model Development*, *10*(4), 1487–1520. <https://doi.org/10.5194/gmd-10-1487-2017>
- Wang, Z. (2013). On the response of Southern Hemisphere subpolar gyres to climate change in coupled climate models. *Journal of Geophysical Research: Oceans*, *118*(3), 1070–1086. <https://doi.org/10.1002/jgrc.20111>
- Williams, C. J. R., Guarino, M.-V., Capron, E., Malmierca-Vallet, I., Singarayer, J. S., Sime, L. C., et al. (2020). CMIP6/PMIP4 simulations of the mid-Holocene and Last Interglacial using HadGEM3: Comparison to the pre-industrial era, previous model versions and proxy data. *Climate of the Past*, *16*(4), 1429–1450. <https://doi.org/10.5194/cp-16-1429-2020>
- Wilson, D. J., Bertram, R. A., Needham, E. F., van de Fliert, T., Welsh, K. J., McKay, R. M., et al. (2018). Ice loss from the East Antarctic Ice Sheet during late Pleistocene interglacials. *Nature*, *561*(7723), 383–386. <https://doi.org/10.1038/s41586-018-0501-8>
- Wu, S., Lembke-Jene, L., Lamy, F., Arz, H. W., Nowaczyk, N., Xiao, W., et al. (2021). Orbital- and millennial-scale Antarctic Circumpolar Current variability in Drake Passage over the past 140,000 years. *Nature Communications*, *12*(1), 3948. <https://doi.org/10.1038/s41467-021-24264-9>